

13.2 EFFECT OF MOIST PROCESSES ON THE FLOW OF AIR WITHIN COMPLEX TERRAIN

Matthias Steiner^{1*} and Richard Rotunno²

¹Princeton University, Princeton, NJ

²National Center for Atmospheric Research, Boulder, CO

1. INTRODUCTION

Analyses of the flow of air within major river valleys on the south side of the European Alps, using ground-based and airborne Doppler radar, surface, and upper-air data taken in the fall of 1999 during the Mesoscale Alpine Program (MAP) Special Observing Period (SOP; Bougeault et al. 2001), show that precipitation can strongly modify the airflow within valleys (Steiner et al. 2003; Bousquet and Smull 2003a, b; Asencio et al. 2004). Observations made during the MAP SOP show that during persistent widespread orographic precipitation events a down-valley drainage flow can develop underneath an opposite-directed flow of moist air that is lifted onto the topographic barrier. Such moist-process-driven drainage flows may reach a maximum depth limited primarily by the height of the melting layer and secondarily by the valley confines. The drainage flow strength and depth are found to be related to the rainfall amount, and within the valley appear to be disconnected from the larger-scale upslope flow (Steiner et al. 2003).

Idealized simulation experiments have been carried out using the new Weather Research and Forecasting (WRF) model (available online at wrf-model.org) to further a fundamental understanding of the effect of atmospheric moisture on the flow of air past a two-dimensional (2D) bell-shaped ridge. Similarly, three-dimensional (3D) simulations have been undertaken with a 2D ridge that included a major valley embedded within. The focus of the analyses is primarily on the characterization of key flow and precipitation features observed on the upstream side of the topographic barrier.

2. NUMERICAL SIMULATION SETTINGS

The simulations have been carried out using version 1.3 of the WRF model in Eulerian mass coordinates (EM core). Only the basic dynamic

and microphysics packages were used, with all other physics packages turned off. Simulations were undertaken with either warm (Kessler 1963) or mixed warm/cold (Lin et al. 1983) microphysics. Only the latter results are discussed here. Fifth- and third-order momentum and scalar advection schemes were used in horizontal and vertical direction, respectively. Open (periodic) boundary conditions were applied in horizontal direction perpendicular (parallel) to the mountain ridge. Rayleigh damping was implemented over the upper 15 km of the 30 km vertical domain. A stretched vertical coordinate system was used, composed of 121 layers. The horizontal domain covered 402 by 3 (2D) and 402 by 22 (3D) grid points at 2 km spacing. In order to ensure quasi-equilibrium flow conditions, the model integration was carried out over 15840 time steps at 10 s (i.e., 44 hours) using a third-order Runge-Kutta scheme.

The terrain was represented by a 2D bell-shaped symmetric ridge with a height of 2500 m and half-widths of 20 (ridge) and 5 (valley) grid points, respectively. The simulations were carried out based on moist neutral soundings (i.e., Brunt-Vaisala frequency $N_m^2 = 0.03 \cdot 10^{-4} \text{ s}^{-2}$), capped by an isothermal layer above the tropopause (200 hPa), with a uniform horizontal wind of $u = 10 \text{ m s}^{-1}$ perpendicular to the ridge and zero along-ridge flow ($v = 0 \text{ m s}^{-1}$). Modifications to the soundings included variations in stability or relative humidity (from dry to saturated conditions), and shifting the entire temperature profile by changing the surface temperature to achieve varying heights of the freezing level relative to the terrain height.

3. IDEALIZED 2D SIMULATIONS

The results of 2D simulations show that moist processes, such as condensation, melting, and evaporation, significantly alter the thermodynamic stratification and stability of the atmosphere, and

* *Corresponding author address:* Dr. Matthias Steiner, Department of Civil and Environmental Engineering, Princeton University, Princeton, New Jersey 08544; phone: 609/258-4614; email: msteiner@princeton.edu

thus modify a flow pattern obtained otherwise based on dry conditions. For example, latent heat released by condensation tends to decrease the thermodynamic stability and thus ease an air parcel to cross over a topographic barrier. Melting and evaporation, on the other hand, result in a cooling of the air that causes subsidence and thus yields increased stability.

A horizontal flow characterized by a saturated moist neutral sounding may surmount a 2500 m high 2D mountain with little flow retardation effect below the crest (Fig. 1 top), while a flow based on a corresponding dry atmosphere is significantly blocked (Fig. 2 top). Increasing the atmospheric stability increases the blocking effect particularly for the saturated moist (Fig. 1 middle and bottom) but less so for the dry (Fig. 2 middle and bottom) simulations. Comparing Fig. 1 (bottom) with Fig. 2 (top) shows that the Brunt-Vaisala frequency has to be approximately five times as large for a saturated moist flow to achieve a comparable blocking effect than for a dry flow over the same topographic barrier (i.e., $N_m \sim 5N_d$).

Alternatively, decreasing the relative humidity of the atmosphere below saturation results in blocking signatures that resemble those of the increased stability simulations (Fig. 1), as shown in Fig. 3. This result is the consequence of a reduced latent heat release to the atmosphere (less moisture available for condensation) and an increasing effect of evaporation of precipitation particles, which tend to increase the atmospheric stability.

The atmospheric stability of moist flow past terrain affects not only the flow patterns but also the spatial distribution and amount of rainfall, as visualized by Figs. 1 and 3, and summarized in Table 1. For example, peak rainfall accumulations are typically found over the mountain slope (i.e., below the crest). Increased blocking effects yield smaller uplift of air and thus reduced amounts of rainfall. The accumulation also drops rapidly with decreasing degree of atmospheric saturation. These results are consistent with those of Colle (2004).

The flow past a 2D bell-shaped mountain and the resulting rainfall depend also on the surface temperature, as shown in Fig. 4 and Table 1. Warmer air may hold more moisture that yields increased rainfall amounts. Flow blocking effects appear to become noticeable particularly once the freezing level sinks below the height of the mountain crest, which tends to trap the air that has been cooled by the melting and evaporation of

falling precipitation particles to the upstream side of the mountain.

The primary difference between simulations with mountain half width of 5 and 20 grid points, respectively, is the significantly increased uplift of air immediately above the mountain slope for the narrower mountain, which results in larger rainfall accumulations, as shown in Table 2. In addition, the narrower mountain exhibits slightly increased upstream blocking effects.

Table 1. Horizontal wind speed at grid point 120 and 400 m altitude (column D; m s^{-1}), maximum rainfall accumulation (column F; mm) and its grid point (column E) for various combinations of atmospheric stability (column A; 10^{-4} s^{-2}), surface temperature (column B; $^{\circ} \text{K}$), and relative humidity (column C). Results are for 44 h simulations with a 2D mountain half width of 20 grid points.

A	B	C	D	E	F
0.03	288	100%	11.1	188	261.7
0.15	288	100%	9.6	189	215.8
0.75	288	100%	-0.5	194	40.3
0.03	288	0%	-0.5		
0.15	288	0%	-0.8		
0.75	288	0%	-0.5		
0.03	288	90%	7.0	185	157.1
0.03	288	80%	2.6	190	86.7
0.03	288	70%	0.7	190	71.0
0.03	278	100%	8.6	189	155.3
0.03	283	100%	9.4	189	214.8
0.03	293	100%	10.5	190	269.0
0.03	298	100%	10.0	191	344.6
0.03	303	100%	10.8	267	379.7

Table 2. Same as Table 1, except for simulations with a 2D mountain half width of 5 grid points.

A	B	C	D	E	F
0.03	288	100%	9.6	197	650.1
0.15	288	100%	9.4	198	541.4
0.75	288	100%	-1.3	199	41.6
0.03	288	0%	-1.3		
0.15	288	0%	-1.2		
0.75	288	0%	-1.2		
0.03	288	90%	7.6	194	412.8
0.03	288	80%	-0.3	199	128.8
0.03	288	70%	-0.7	199	87.6
0.03	278	100%	9.4	198	422.1
0.03	283	100%	9.4	197	589.1
0.03	293	100%	9.9	198	750.7
0.03	298	100%	9.6	198	959.3
0.03	303	100%	9.7	198	533.3

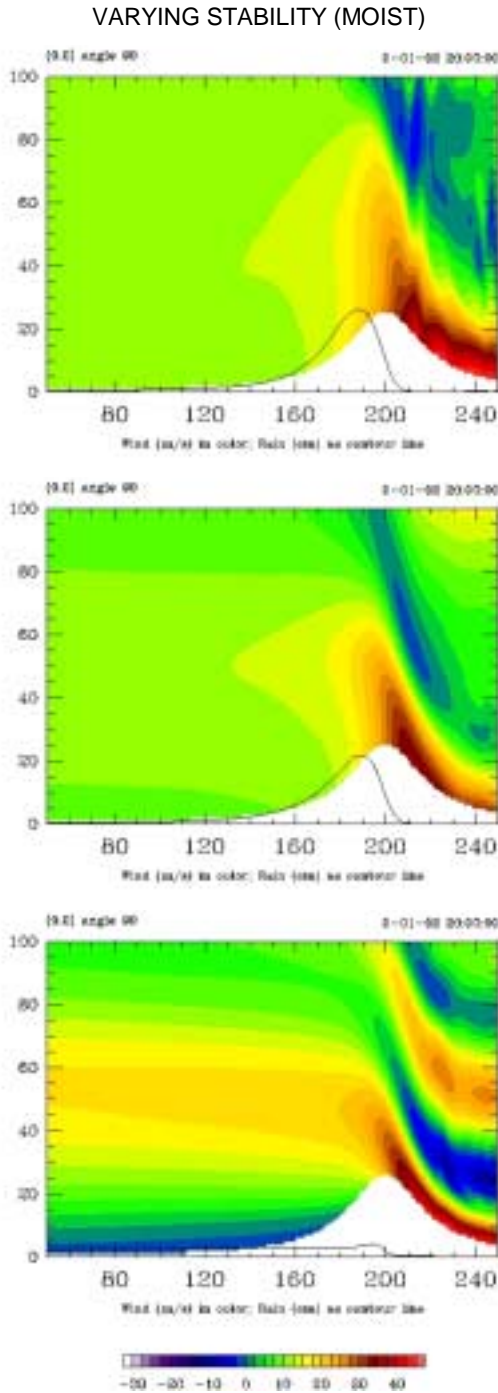


Fig. 1. WRF model simulations of the horizontal flow field (in color) and rainfall accumulation (solid line) past a 2D mountain based on a surface temperature of 288° K and soundings of a varying degree of stability: moist neutral with $N_m^2 = 0.03 \cdot 10^{-4} \text{ s}^{-2}$ (top), $N_m^2 = 0.15 \cdot 10^{-4} \text{ s}^{-2}$ (middle), and $N_m^2 = 0.75 \cdot 10^{-4} \text{ s}^{-2}$ (bottom). Results are for Lin et al. (1983) ice microphysics. The axes are grid points in horizontal and hectometers (cm for rain) in vertical direction.

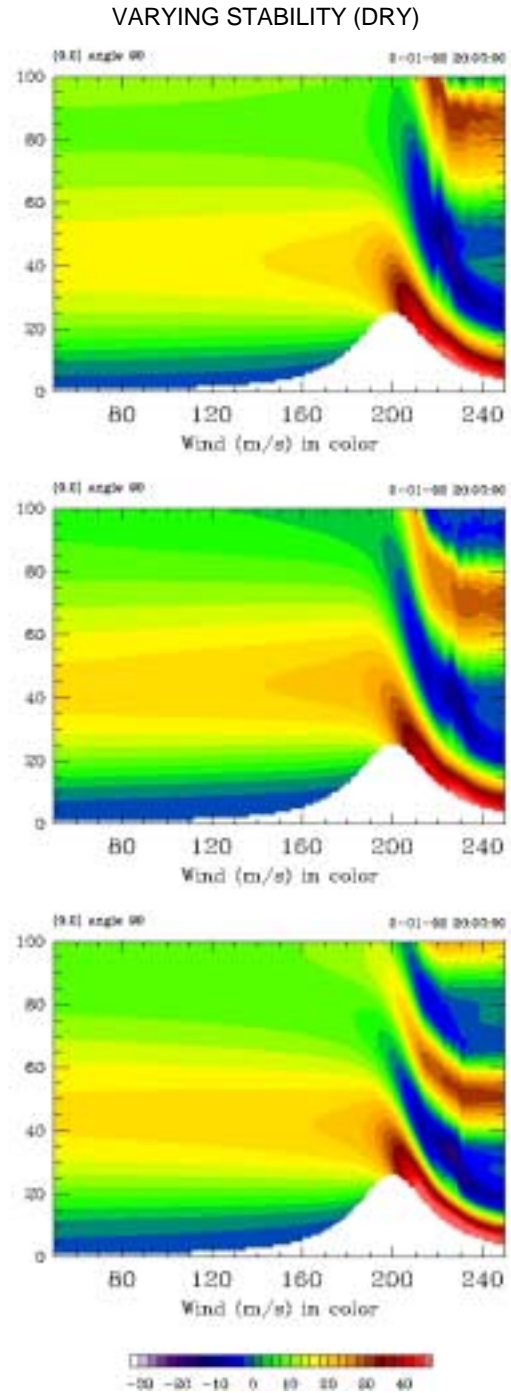


Fig. 2. WRF model simulations of the horizontal flow field (in color) past a 2D mountain based on a surface temperature of 288° K and soundings of a varying degree of stability: moist neutral with $N_m^2 = 0.03 \cdot 10^{-4} \text{ s}^{-2}$ (top), $N_m^2 = 0.15 \cdot 10^{-4} \text{ s}^{-2}$ (middle), and $N_m^2 = 0.75 \cdot 10^{-4} \text{ s}^{-2}$ (bottom). The simulations are with all moisture removed (dry). The axes are grid points in horizontal and hectometers in vertical direction.

VARYING SATURATION

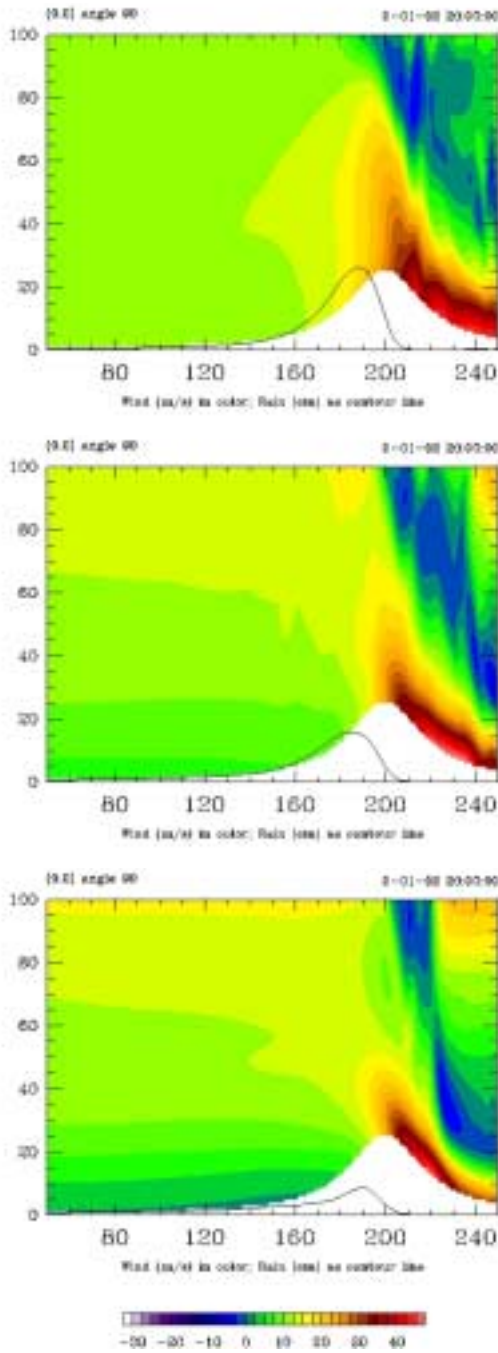


Fig. 3. WRF model simulations of the horizontal flow field (in color) and rainfall accumulation (solid line) past a 2D mountain based on a surface temperature of 288° K and a moist neutral sounding with 100% (top), 90% (middle), and 80% (bottom) saturation. Results are for Lin et al. (1983) ice microphysics. The axes are grid points in horizontal and hectometers (cm for rain) in vertical direction.

VARYING SURFACE TEMPERATURE

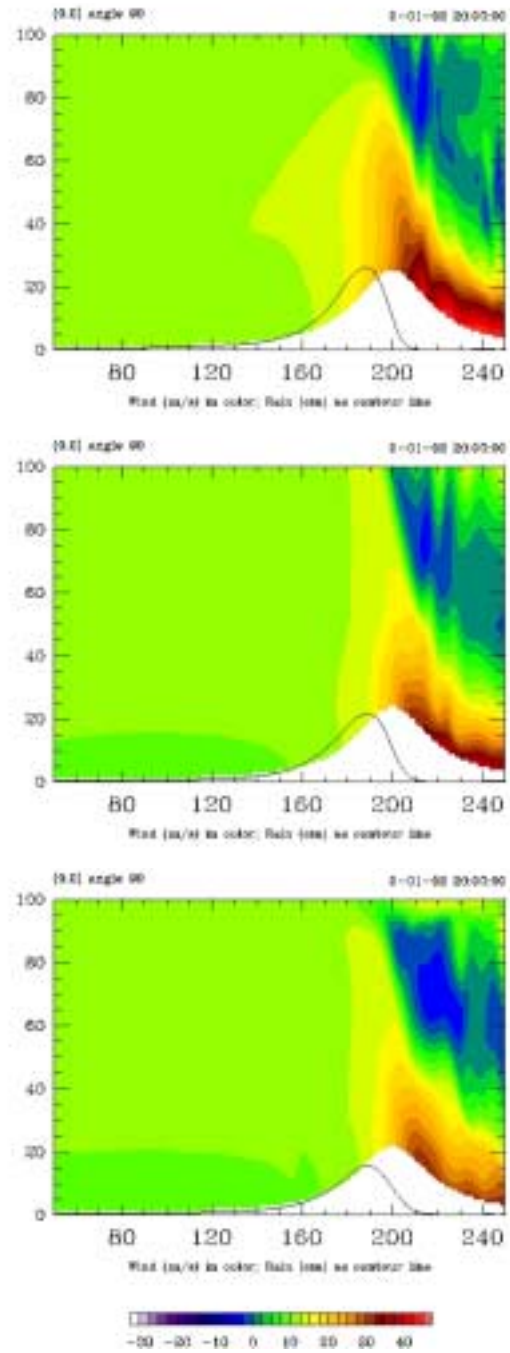


Fig. 4. WRF model simulations of the horizontal flow field (in color) and rainfall accumulation (solid line) past a 2D mountain based on a saturated moist neutral sounding and surface temperatures of 288° K (top), 283° K (middle), and 278° K (bottom). Results are for Lin et al. (1983) ice microphysics. The axes are grid points in horizontal and hectometers (cm for rain) in vertical direction.

4. IDEALIZED 3D SIMULATIONS

Building on the 2D analyses discussed before, fully 3D simulations have been carried out for flow over topography that contained a major valley embedded within an otherwise straight ridge, as depicted in Fig. 5. The mountain half widths are 20 and 5 grid points for the ridge and valley, respectively, with linearly sloping valley sidewalls.

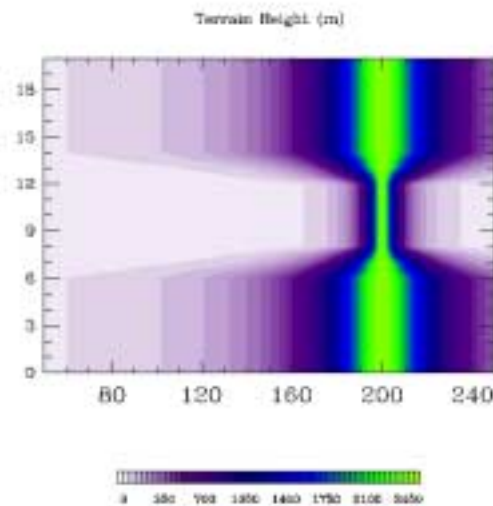


Fig. 5. Topography used for the WRF model simulations. The terrain height is shown in colors. The axes are grid points.

Figure 6 shows vertical cross sections of the along-domain flow field after 20 h of simulation at the edge (ridge) and center (valley) of the domain. There are significant differences between the 3D (shown in colors) and 2D simulations, as indicated by the contours. The upslope flow in the 3D simulation is stronger above the terrain slope, especially so within the valley. A horizontal flow convergence is found over the valley's sidewalls near the crest of the mountain (top panel of Fig. 7), causing enhanced updrafts. This couplet of updrafts, as depicted in Fig. 8, is responsible for the rainfall distribution shown in the bottom panel of Fig. 7. Subsidence occurs over the center of the valley that suppresses precipitation formation but also enhances the down-slope and down-valley flow seen in Fig. 6 (bottom panel). Although the simulation hasn't reached steady state yet after 20 h, it appears as if the blocked and reversing flow within the valley confines forms a cushion of air that tends to fill the gap created within the ridge by the valley. Such a feature is not seen in the corresponding 2D simulations.

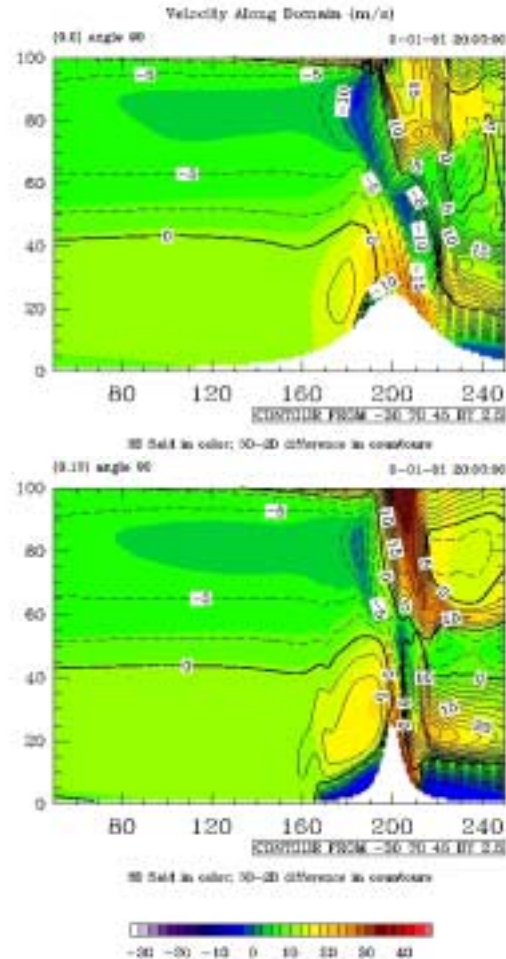


Fig. 6. WRF model simulations of the along-domain flow field (in color) past the terrain shown in Fig. 5 and difference between the 3D and 2D simulations (in contours) based on a saturated moist neutral sounding and surface temperatures of 288° K. Results are shown at the edge of the domain (top panel) and in the center of the valley (bottom panel) after 20 hrs of simulation with the Lin et al. (1983) ice microphysics. The axes are grid points in horizontal and hectometers in vertical direction.

5. SUMMARY

Simulations using the new Weather Research and Forecasting (WRF) model show that moist processes have a profound effect on flow past 2D bell-shaped mountains and 3D ridges containing a major embedded valley. Effects of atmospheric stability, degree of saturation, and freezing level height have been investigated from a perspective of the flow upstream of a topographic barrier. Simulations based on major valleys embedded

within otherwise straight ridges highlight significant 3D effects on the flow past the terrain that determine the spatial rainfall distribution. The reverse flow seen within a valley is markedly different from a flow that would be observed for a 2D ridge with the same half width as the terrain at the upper end of the valley.

Additional analyses have to be carried out to further digest these simulations, and also to study the effect of the valley geometry in the flow and spatial rainfall distribution.

Acknowledgments. The WRF-related, excellent assistance provided by William Skamarock, David Gill, John Michalakes, Wei Wang, and Jimmy Dudhia of the National Center for Atmospheric Research (NCAR) is much appreciated. The first author is grateful to multiple visiting appointments with the Mesoscale and Microscale Meteorology (MMM) Division of NCAR. This research project has been supported by the National Science Foundation (NSF) Grant ATM-9906012 through the Mesoscale Dynamic Meteorology Program managed by Dr. Stephan Nelson.

REFERENCES

- Asencio, N., J. Stein, and M. Chong, 2004: Comparison of the down-valley flow for the MAP IOP 8 and IOP 3 with the numerical laboratory MesoNH model. *11th Conference on Mountain Meteorology and Annual MAP Meeting*, Mount Washington Valley, New Hampshire, Amer. Meteor. Soc., paper 12.6.
- Bougeault, P., P. Binder, A. Buzzi, R. Dirks, R. Houze, J. Kuettner, R. B. Smith, R. Steinacker, and H. Volkert, 2001: The MAP Special Observing Period. *Bull. Amer. Meteor. Soc.*, **82**, 433-462.
- Bousquet, O., and B. F. Smull, 2003a: Observations and impacts of upstream blocking during a widespread orographic precipitation event. *Quart. J. Roy. Meteor. Soc.*, **129**, 391-409.
- Bousquet, O., and B. F. Smull, 2003b: Airflow and precipitation fields within deep Alpine valleys observed by airborne Doppler radar. *J. Appl. Meteor.*, **42**, 1497-1513.
- Colle, B. A., 2004: Sensitivity of orographic precipitation to changing ambient conditions and terrain geometries: An idealized modeling perspective. *J. Atmos. Sci.*, **61**, 588-606.
- Kessler, E., 1963: Elementary theory of associations between atmospheric motions and distributions of water content. *Mon. Wea. Rev.*, **91**, 13-27.
- Lin, Y.-L., R. D. Farley, and H. D. Orville, 1983: Bulk parameterization of the snow field in a cloud model. *J. Clim. Appl. Meteor.*, **22**, 1065-1092.
- Steiner, M., O. Bousquet, R. A. Houze Jr., B. F. Smull, and M. Mancini, 2003: Airflow within major Alpine river valleys under heavy rainfall. *Quart. J. Roy. Meteor. Soc.*, **129**, 411-431.

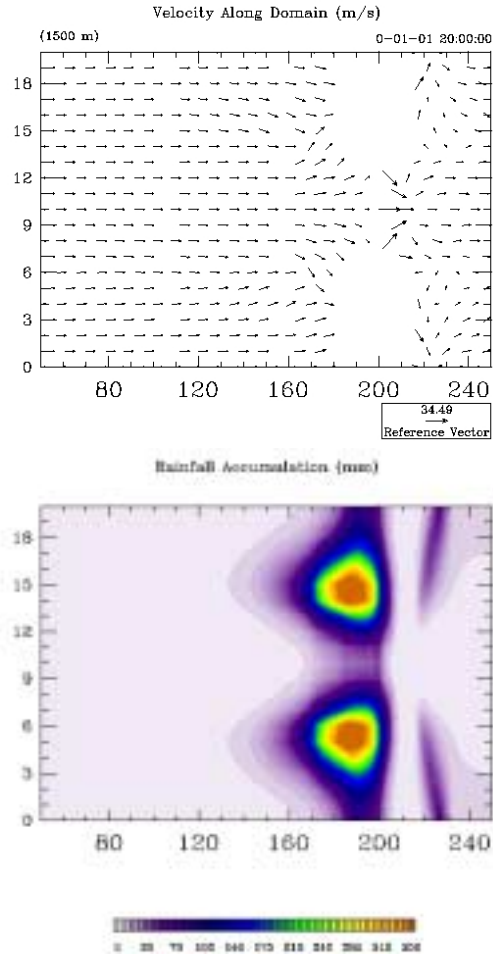


Fig. 7. WRF model simulations of the horizontal flow field at 1500 m (top panel) and rainfall accumulation (bottom panel) corresponding to the results shown in Fig. 6. The axes are grid points.

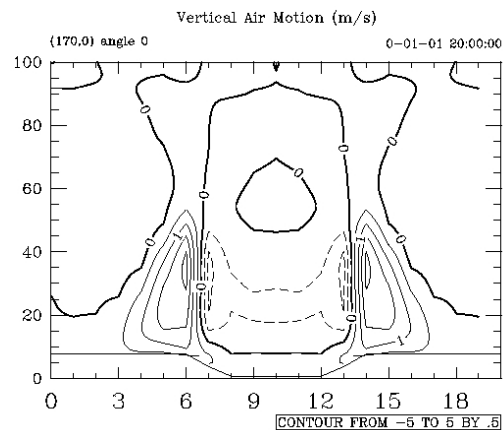


Fig. 8. Vertical air motions within a vertical cross section parallel to the ridge at grid point 170 based on the WRF model simulation depicted in Figs. 6 and 7. The axes are grid points in horizontal and hectometers in vertical direction.